Mild Steel Corrosion Inhibition by Furocoumarin Derivatives in Acidic Media

H. Lgaz[1], S. Zehra[2], K. Toumiat[3], A. Chaouiki[4], Y. El Aoufir[5], Ismat. H. Ali[6], M. I. Khan[7], R. Salghi[4,*], I-M. Chung[1,*]

[1] Department of Crop Science, College of Sanghur Life Science, Konkuk University, Seoul 05029, South Korea
[2] Corrosion Research Laboratory, Department of Applied Chemistry, Faculty of Engineering and Technology, Aligarh Muslim University, Aligarh, India
[3] Department of Materials Sciences, Laghouat University, PO Box 37, 03000, Laghouat, Algeria
[4] Team of Applied Chemistry and Environment, ENSA, University Ibn Zohr, PO Box 1136, Agadir, Morocco
[5] Materials, Nanotechnology and Environment Laboratory, Faculty of Sciences, Mohammed V University Rabat, Morocco.
[6] Department of Chemistry, College of Science, King Khalid University, P. O. Box 9004, Postal Code 61413, Abha, Kingdom of Saudi Arabia
[7] Chemical Engineering Department, College of Engineering, King Khalid University, Abha, Kingdom of Saudi Arabia
[*]E-mail: r.salghi@uiz.ac.ma, imcim@konkuk.ac.kr,

The development of natural-based corrosion inhibitors has increasingly become an important research objective. Herein, we report the potential use of two natural furocoumarins namely, Bergamottin (FC-C) and Isopimpinellin (FC-M) for the corrosion protection of mild steel (MS) in 1.0 M HCl. Corrosion inhibitory activities of two compounds were evaluated using gravimetric, electrochemical, scanning electron microscope (SEM) and computational techniques. Electrochemical results disclosed that the two compounds could effectively control the dissolution rate of mild steel in acidic medium through physicochemical adsorption following Langmuir adsorption model. Potentiodynamic polarization curves indicated that the furocoumarin molecules could be classified as mixed-type inhibitors by preventing anodic metal dissolution and cathodic hydrogen evolution reaction. Density functional theory (DFT) and molecular dynamics (MD) simulations were carried out to describe electronic properties of two furocoumarins and their interaction with Fe(110) surface.

Keywords: Mild steel; Corrosion inhibition; HCl; Furocoumarin; Molecular dynamic; DFT.

1. INTRODUCTION

Corrosion of metals is one of the most challenging tasks that needed sustained attention and development of more efficient processing for preventing or controlling metal's damage [1–6]. Mild steel is a familiar material employed in a wide range of structural and industrial applications, including chemical and petroleum refining industries [7]. In several industrial processes such as acid pickling of steel, industrial cleaning, and oil-well acidization, etc. mineral acids, particularly hydrochloric acid, are frequently used, in which, steel undergoes severe corrosion.

In hope of reducing the economic effect of corrosion, which costs around $4 trillion a year globally, a continuing effort has been made to diagnose, evaluate and control corrosion issues [8]. Organic corrosion inhibitors are currently one of the most popular and practical methods for improving the corrosion resistance properties of metals, especially in acidic environments [9–15]. Data from several studies suggest that most of organic compounds being used as inhibitors of corrosion act by adsorption on the surface of the metal. The extent of adsorption of an organic compound on the metal surface is first and foremost influenced by its physicochemical properties, which in turn depend on the presence of heteroatoms such as N, S and O, functional groups, and steric factors, among others [16,17]. Over the last years, several researches have been conducted using a diverse class of organic compounds as corrosion inhibitors. Nowadays, efforts have been made in search of potent green corrosion inhibitors because the importance of environmental protection has become increasingly recognized and appreciated. Recently, several comprehensive reviews summarized the ongoing efforts and the developments in this field [18–20].

Complementary to the experimental approach, recent advances in computational hardware and software have enabled the large-scale prediction of inhibitor-metal interactions and have led to explore unknown properties at the molecular level. Computational chemistry involving DFT calculations and MD simulations are of important significance to explore the inhibition mechanism[21]. Density Functional Theory is currently the most popular method for investigating the chemical reactivity of isolated inhibitor molecules. Meanwhile, molecular dynamics (MD) simulations, have been successful in predicting and analyzing the adsorption behavior of corrosion inhibitor molecules[22]. The main advantage of this method is that it can provide further insights into the adsorption process in presence of the most corrosive environment factors, such as solvent, temperature and pressure, etc.[23].

In this work, our aim object is to have a basic knowledge of the corrosion inhibition behavior and the adsorption of two natural compounds, i.e. bergamottin and isopimpinellin, on the mild steel surface immersed in 1.0 M HCl. Bergamottin and isopimpinellin are natural organic compounds of the class of furocoumarins[24,25]. Bergamottin is present mainly in grapefruit juice. It is also found in the essential oil of bergamot, from which it is isolated and from which its name is derived. Isopimpinellin, on the other hand, is found in *S. moellendorffii*[26], it was previously reported to be sporadically distributed in flowering plants[27,28]. Several studies have been carried out to investigate the effects of isopimpinellin and bergamottin as anticancer agents[28,29].
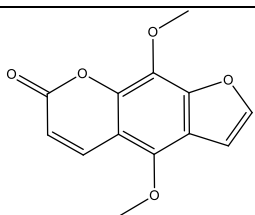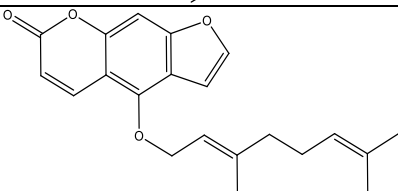
Electrochemical and surface characterization techniques were implemented to investigate the performance of the two furocoumarins for inhibiting the mild steel corrosion in 1.0 M HCl. Afterward; computational techniques were successfully used to theoretically explain corrosion inhibition mechanisms.

2. EXPERIMENTAL

2.1. Materials and corrosive solutions

The chemical composition of metal substrates was: 0.36 wt.% C, 0.66 wt.% Mn, 0.27 wt.% Si, 0.02 wt.% S, 0.015 wt.% P, 0.21 wt.% Cr, 0.02 wt.% Mo, 0.22 wt.% Cu, 0.06 wt.% Al and balance Fe. Surface of working electrode (MS specimens) were grated with different degrees of granulation of abrasive papers (SiC; 600-1600), and to eliminate the abrasion products, the abraded specimens were cleansed with bidistilled water, then with acetone, and eventually dried at room temperature. The test solution employed (HCl of 1.0 M concentation) was prepared from the commercially obtained 37% HCl, by diluting with aid of distilled water. Isopimpinellin and bergamottin are purchased from Sigma-Aldrich and used without any further purification (Table 1).

Table 1. Chemical names and structures of furocoumarin derivatives.

Furocoumarin derivatives	Structure	Notation
Isopimpinellin		FC-M
Bergamottin		FC-C

Inhibitor stock solutions of 5×10^{-4} M were prepared in 1.0 M HCl and the other concentrations were obtained by serial dilution of the stock solution. The range of concentrations of employed inhibitors was kept in between 1×10^{-5} to 5×10^{-4} M. No significant results were found for the other concentrations.

2.2. Weight loss measurements

Traditional weight loss immersion tests were performed to measure and compare the corrosion rate of the mild steel in different inhibitor concentrations. Prior to each individual experiment, the mild steel samples were prepared as described above. The samples were weighed using a precision weighing balance (precise to 0.1 mg) and immersed in blank and inhibited solutions for 24h at 303K. The mild steel samples were weighed again accurately after a complete washing, cleaning and drying process. For each concentration, triplicates measurements were carried out. All tests were performed respecting the standard laboratory methodology adopted by the ASTM [30]. The corrosion rate (C_{RW}) in millimeters per year (mm y^{-1}) was calculated by dividing the mass loss (W) in gram by the exposed area (A) in cm^2, density (7.86 g cm^{-3}) [31], and time of exposure in hours using the following equation [32]:

$$C_{RW} = \frac{K \times W}{A \times t \times \rho}$$ (1)

where K= 8.76×10^4 was used as constant.

2.3. Electrochemical measurements

Electrochemical experiments were carried out by using an electrochemical workstation (Tacussel Radiometer PGZ 100 potentiostat) controlled by VoltaMaster software, and a cell of glass with three electrode assembly consisting of MS as working electrode (1 cm^2 dimension), platinum electrode as counter electrode, and a saturated calomel electrode (SCE) as the reference electrode. The working electrode was immersed in the aggressive test solution for 30 min at 303 K, prior to the tests. Measurements were performed only when there was a steady state open circuit potential. EIS tests were carried out by the application of peak-to-peak perturbations of 5 mV, at open circuit potential in the frequency range 10 mHz to 100 KHz. PDP curves reported here were obtained at a scan rate of 1 mVs^{-1} by automatically sweeping the applied electrode potential from −800 to -200 mV vs. OCP. Tafel extrapolation method was used to extract electrochemical parameters at ±50 mV around E_{corr} [33]. All experiments were carried out under aerated unstirred conditions at 303 K.

2.4. Computational chemical details

2.4.1. DFT calculations

Our approach to the corrosion inhibition process is interdisciplinary and by combining experimental and theoretical investigations. Quantum chemical calculation were accomplished by acquiring complete geometry optimization using Gaussian 09 W software for Windows [34,35] by using DFT at the 6-311++G(d, p) basis set for all atoms. The aqueous phase model was the Self-Consistent Reaction Field (SCRF) theory, with Polarized Continuum Model (PCM)[36]. The ionization potential (I) and the electron affinity (A) are given based on the eigenvalue of HOMO and LUMO orbitals as a result of Koopmans's theorem by using following equations [37,38]:

The electron affinity (EA) $EA = -E_{LUMO}$ (2)

The ionization potential (IP) $IP = -E_{HOMO}$ (3)

Chemical hardness (η), Mulliken electronegativity (χ), and fraction of electrons transferred (ΔN) from inhibitor to metallic surface can be approximated using the equations [26,27]:

$$\eta = \frac{IP - EA}{2}$$ (4)

$$\chi = \frac{IP + EA}{2}$$ (5)

$$\Delta N = \frac{\phi - \chi_{inh}}{2(\eta_{Fe} + \eta_{inh})}$$ (6)

where (ϕ=4.82) is the work function of the Fe(110) while $\eta_{Fe} = 0$ is the chemical hardness of iron [39,40].

The Fukui functions were calculated based on Hirschfeld population analysis (HPA). Gradient-corrected exchange and correlation functionals (GGA-PBE) in combination with the double numerical plus polarization (DNP) basis set are applied for all atoms. Dmol^3 code implemented in Material Studio[41] was used for all Fukui functions calculations. In Fukui functions calculations, the potential electrophilic and nucleophilic atoms were identified as follows [42]:

$$f_k^+ = q_k(N+1) - q_k(N) \tag{7}$$

$$f_k^- = q_k(N) - q_k(N-1) \tag{8}$$

where q_k is the electronic population of an atomic site within a molecule in its neutral (N), anionic (N+1) or cationic (N-1) state [43].

2.4.2. Molecular dynamics (MD) simulations

Molecular dynamics simulation (MD) was performed using Materials studio package [1]. The solvent layer that contains water molecules (491), chlorine and hydronium ions (9) along with an inhibitor molecule was collected with the iron layer in one simulation box (24.82×24.82×35.69 Å^3) and optimized before MD simulation [14]. The COMPASS force field [15] and the NVT canonical ensemble were used for all simulations. The simulations were completed in a time step of 1 fs and simulation time of 2000 ps at 303 K [16]. When the system reaches the equilibrium state, the interaction and the binding energies ($E_{Binding} = -E_{interaction}$) were estimated by applying the following equation [17]:

$$E_{interaction} = E_{total} - (E_{surface+solution} + E_{inhibitor}) \tag{9}$$

In the above equation, $E_{surface+solution}$ denotes the total energy of the Fe(110) and solution without inhibitor molecule, $E_{inhibitor}$ refers to the total energy of an inhibitor molecule alone and E_{total} denotes the total energy of the full system.

Radial distribution function (RDF) was analyzed from MD trajectory data. The RDF is defined by Hansen and McDonald as[47]:

$$g_{AB}(r) = \frac{1}{\langle \rho_B \rangle_{local}} \times \frac{1}{N_A} \sum_{i \in A}^{N_A} \sum_{j \in B}^{N_B} \frac{\delta(r_{ij} - r)}{4\pi r^2} \tag{10}$$

Where $\rho_{B\,local}$ represents the particle density of B averaged over all shells around particle A.

2.5. Surface characterization

Mild steel samples were immersed in 1.0 M HCl without and with 5×10^{-4} M of FC-M for 24h and observed under SEM using a Hitachi TM-1000.

3. RESULTS AND DISCUSSION

3.1. Potentiodynamic polarization curves

It is recognized that the simultaneous anodic and cathodic half–reactions which occur during a potential scan lead to the formation of a corrosion product layer, and its characteristics influence the properties of the polarization curve and its derivable parameters [48]. Figure 1 shows the PDP profiles of the mild steel electrode in 1.0 M HCl in the presence and absence of inhibitors at 303 K.
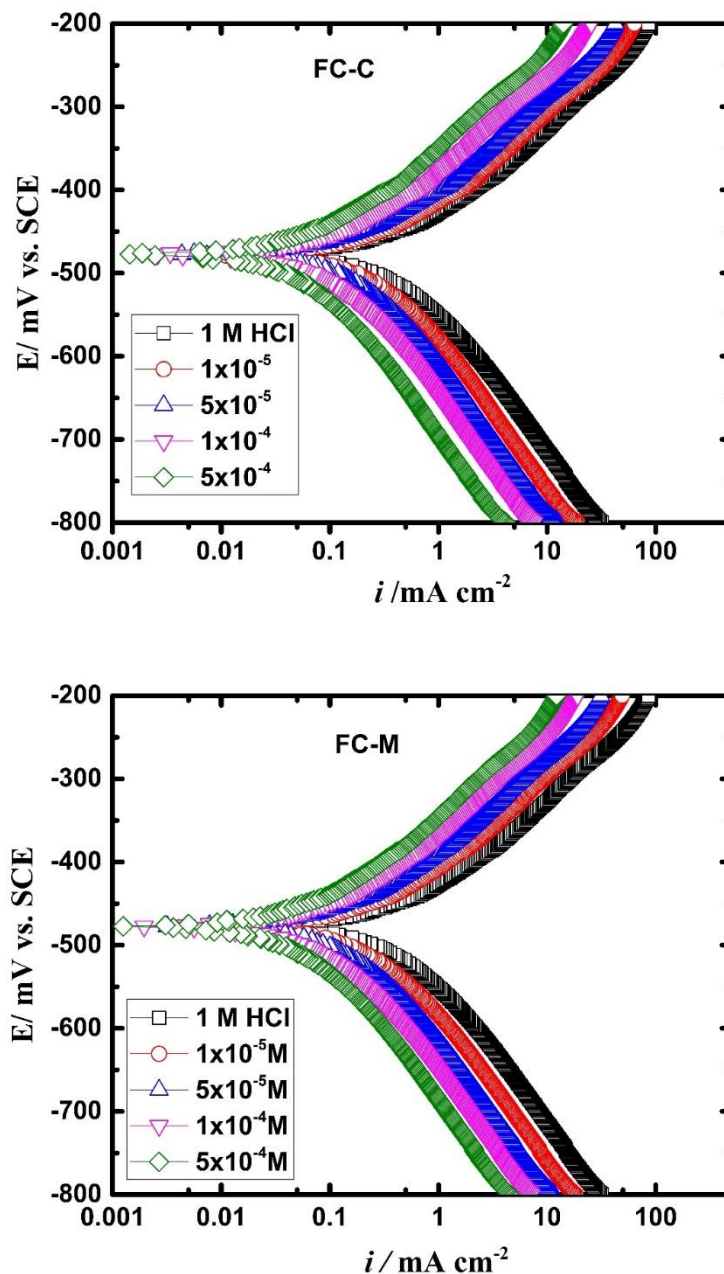
Figure 1. PDP curves of mild steel in 1.0 M HCl with and without inhibitor concentrations at 303 K.

Inhibition efficiency values and electrochemical kinetic parameters are listed in Table 2. The equation 12 was used to determine the inhibition efficiency:

$$\eta_{PDP}(\%) = \left[1 - \frac{i_{corr}}{i_{corr}^{\circ}} \right] \times 100 \tag{12}$$

where i_{corr} and i_{corr}° are the corrosion current densities under inhibited and uninhibited conditions, respectively.

Table 2. Parameters of PDP of the MS in uninhibited and inhibited solutions at 303 K.

Inhibitors	Concentration/ M	$-E_{corr}$ / mVvs. SCE	$-\beta_c$ / mV dec^{-1}	β_a / mV dec^{-1}	i_{corr} / μA cm^{-2}	η_{PDP} / %	Θ
HCl	1.0	480	175	116	481	-	-
FC-C	1×10^{-5}	481	176	115	240	50	0.50
	5×10^{-5}	480	173	114	180	62	0.62
	1×10^{-4}	479	174	116	110	77	0.77
	5×10^{-4}	481	177	117	70	85	0.85
FC-M	1×10^{-5}	479	177	114	220	54	0.54
	5×10^{-5}	481	176	117	150	69	0.69
	1×10^{-4}	481	177	116	90	81	0.81
	5×10^{-4}	480	175	115	50	90	0.90

Looking at Figure 1 and considering the results in Table 2, we can see that there was a significant decrease in i_{corr} values on the addition of furocoumarins concentration in HCl medium. Furthermore, no significant changes can be observed in corrosion potential values as well as in anodic and cathodic Tafel slopes and both remain almost unchanged. Overall, these results indicate that the addition of each inhibitor effectively retarded the hydrogen evolution and suppressed the anodic dissolution without changing the mechanism of corrosion process[49] from which it can be concluded that these compounds are mixed type inhibitors. Consistent with the literature, the mode of inhibition is based on geometric blocking effect whose the compounds act as "adsorptive inhibitors"[32]. That is to say, inhibitors hinder the release of hydrogen gas and reduce anodic dissolution via blocking the active reaction sites on the surface of the mild steel. They can also screen the covered part of the electrode and therefore protect it from the action of the corrosion medium[50].

Based on the data from Table 2, the higher increase of inhibition efficiency values of both inhibitors when increasing their concentration can generally be explained by the significant increase in inhibitor-metal interactions and percentage of surface covered by molecules.

3.2. Electrochemical impedance spectroscopy measurements

The information concerning the mechanism and rate of charge transfer both at uninhibited and inhibited solutions can be provided by the EIS characterization at OCP [50]. The EIS results have been represented in the Nyquist, Bode phase angle and Bode modulus formats, as shown in Figure 2 and 3. At higher frequency region, the plots exhibited one single capacitive loop somewhat depressed at the center which signified that corrosion of mild steel in 1.0 M HCl solution is mainly governed by charge transfer mechanism [51].
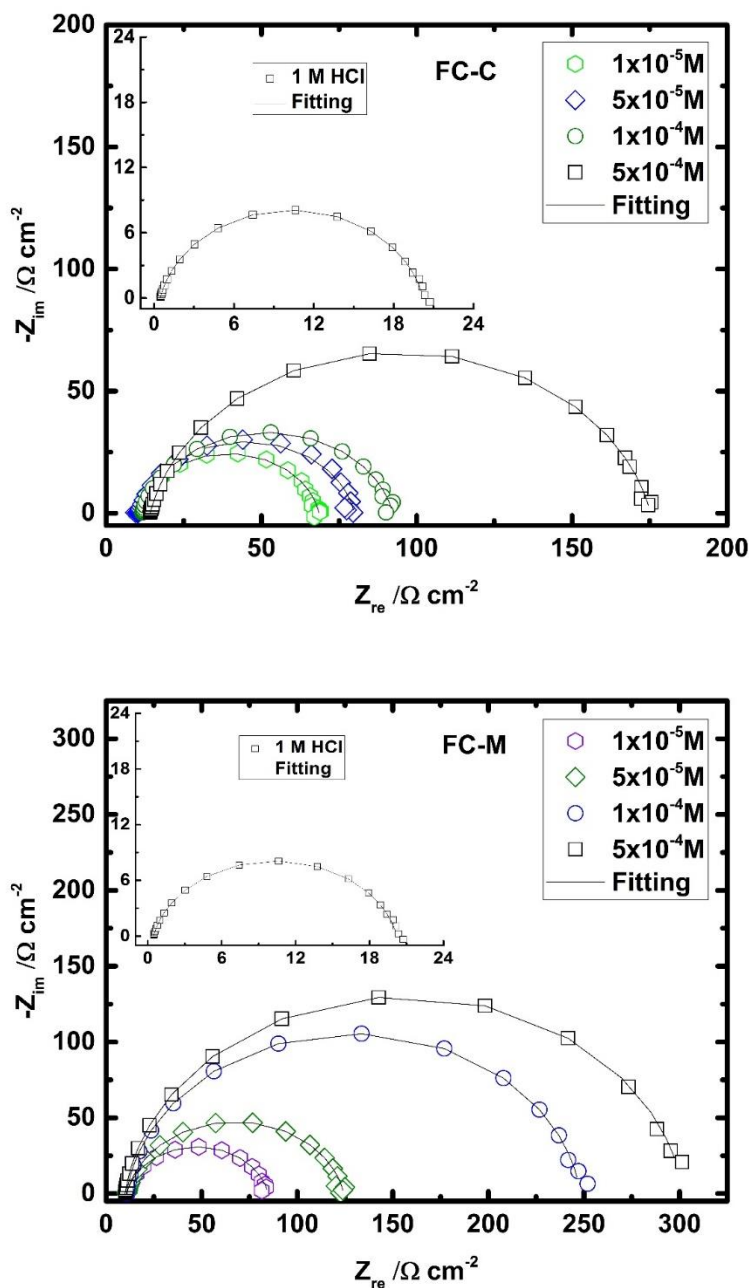
Figure 2. Nyquist diagrams of mild steel in 1.0 M HCl with and without inhibitor concentrations at 303 K.

The equivalent circuit used to fit the impedance data is presented in Figure 4 and the corresponding electrochemical parameters along with the inhibition efficiency are listed in Table 3. The impedance data were fitted to the electrical equivalent circuit shown in Figure 4 to extract the impedance parameters from the experimental results [37,38]. More details on the CPE and the used equivalent circuit model are given in our previous works [39].

Herein, the effective double layer (C_{dl}) values are obtained using the following relationship [53,54]:

$$C_{dl} = \left(Q R_p^{1-n} \right)^{1/n} \tag{13}$$

The following equation was used to estimate the inhibition efficiency [55]:

$$\eta_{EIS}(\%) = \left[\frac{R_{p(inh)} - R_p}{R_{p(inh)}} \right] \times 100 \tag{14}$$

where, $R_{p(inh)}$ and R_p are polarization resistances with and without furocoumarins, respectively.

Table 3. Impedance parameters for corrosion of MS in uninhibited and inhibited solutions at 303 K.

Inhibitors	Concentration/ M	R_p/ Ω cm^2	n	$Q \times 10^{-4}$/ S^n Ω^{-1} cm^{-2}	C_{dl}/ μF cm^{-2}	η_{EIS}/ %
Blank	1.0	20.24	0.860	2.420	112.04	-
	1×10^{-5}	58	0.88	0.9079	44	65
FC-C	5×10^{-5}	70	0.89	0.7012	36	71
	1×10^{-4}	81	0.87	0.6901	31	75
	5×10^{-4}	161	0.87	0.5175	25	87
	1×10^{-5}	73	0.88	0.7317	35	72
FC-M	5×10^{-5}	113	0.86	0.6134	27	82
	1×10^{-4}	237	0.85	0.4844	22	91
	5×10^{-4}	292	0.86	0.3977	19	93

The data depicted in Table 3 revealed that R_p values increased with simultaneous decrease in the C_{dl} with the addition of inhibitors in aggressive test solution as compared to blank test solution. Increase in R_p values is indicative of the adhered inhibitor molecules, thus forming an insulating protective barrier film onto the mild steel surface while the decrease in C_{dl} could be ascribed either to the decreased dielectric constant values, or the increased double layer thickness, or both, occurring simultaneously [56]. To conclude, these results strengthen the idea that tested compounds act just via an effective adsorption at the interface between the metal and the solution i.e, as adsorptive inhibitors. If this is the case, then it seems reasonable to assume that the adsorption of inhibitor molecules is directly influenced by the increase in polarization resistance.
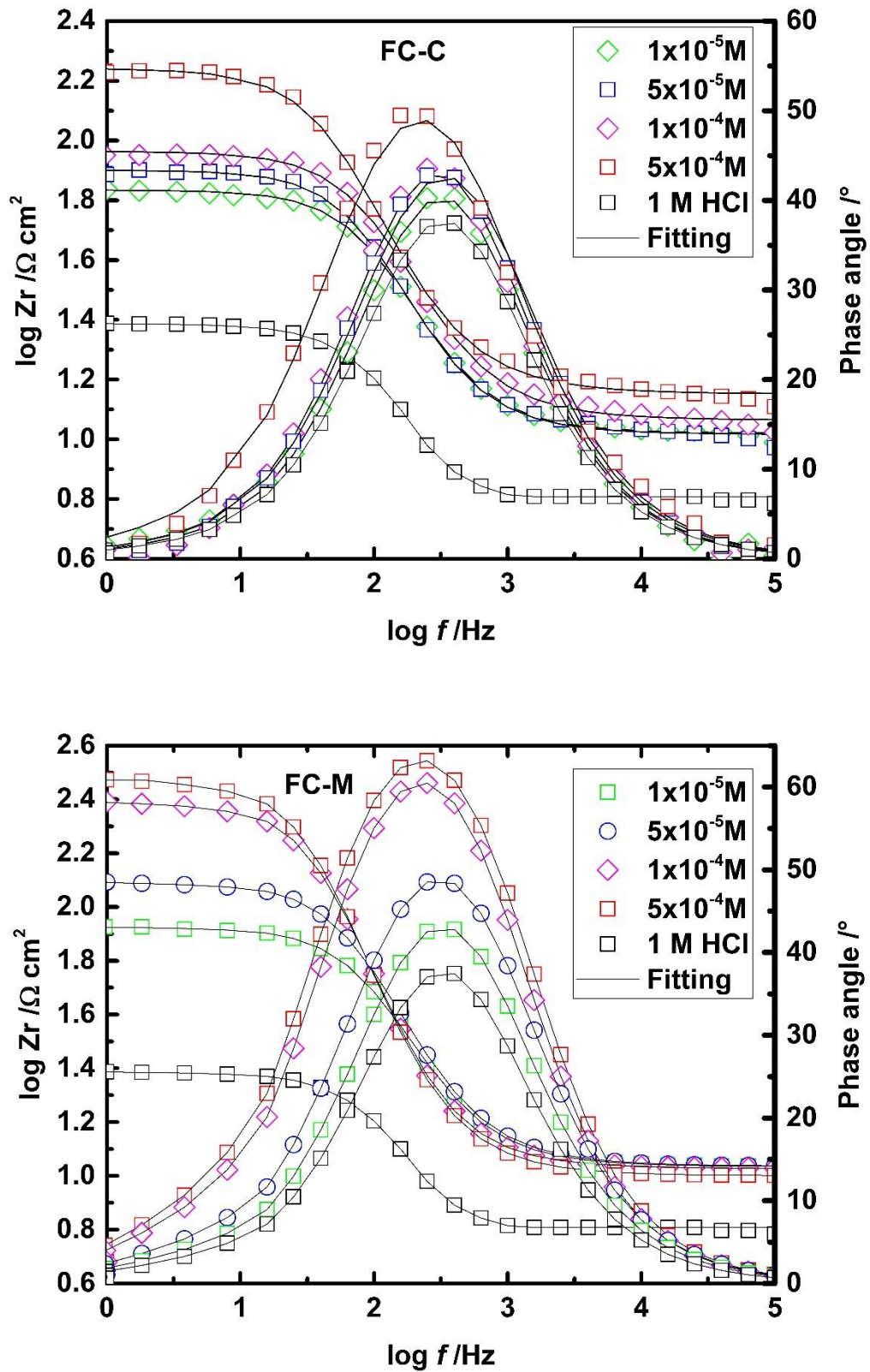
Figure 3. Bode (log *f vs.* log |Z|) and phase angle (log *f vs.* Φ) plots of impendence spectra for MS in 1.0 M HCl containing different concentrations of inhibitors.
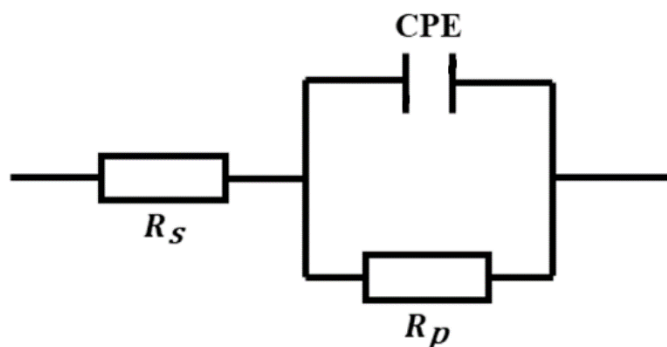
Figure 4. The electrical equivalent circuit.

3.3. Weight loss measurements

The loss in the weight of MS pieces in uninhibited and inhibited solutions was determined. The inhibition efficiency ($\eta_{WL}(\%)$) and surface coverage (θ) are obtained using following equations [57]:

$$\eta_{WL}(\%) = \left[\frac{C^\circ_{RW} - C_{RW}}{C^\circ_{RW}} \right] \times 100 \tag{15}$$

$$\theta = \left[\frac{C^\circ_{RW} - C_{RW}}{C^\circ_{RW}} \right] \tag{16}$$

Where C°_{RW} and C_{RW} are corrosion rates before and after addition of the inhibitor, respectively.

The obtained results are presented in Table 4. Inhibitor molecules protect the mild steel sample through effective adsorption on its surface. As a result, a drastic decrease in the corrosion rate was observed. The resulting decrease in corrosion rate at a relatively small inhibitor concentration allows us to conclude that these compounds have a strong protective effect. This conclusion would then greatly support the assumption that the corrosion attack is greatly suppressed when inhibitor molecules adsorbed on the metal surface, which is believed to closely relate with the charge transfer between iron atoms and adsorbed molecules. In acidic medium, protonated molecules can strongly increase the interaction with the steel surface through physical interactions.

Table 4. Weight loss data of MS in uninhibited and inhibited solutions at 303 K.

Inhibitors	Concentration/ M	C_{RW}/ mm y^{-1}	η_{WL}/ %
HCl	1	130.4	-
FC-C	1×10^{-5}	55.3	57
	5×10^{-5}	41.6	68
	1×10^{-4}	36.1	72
	5×10^{-4}	21.8	83
FC-M	1×10^{-5}	47.5	63
	5×10^{-5}	31.9	75
	1×10^{-4}	18.5	86
	5×10^{-4}	11.6	91

3.4. Adsorption isotherm

After calculating the electrochemical parameters for the two compounds, adsorption isotherms were used to evaluate the interaction of the inhibitor molecule with the metallic surface [50]. The surface coverage values obtained from weight loss measurement were used to fit different adsorption isotherms such as Langmuir, Temkin, Frumkin *etc*. It is found that among these adsorption isotherm models, Langmuir adsorption isotherm (Figure 5) fitted well with regression coefficient (R^2) close to unity.
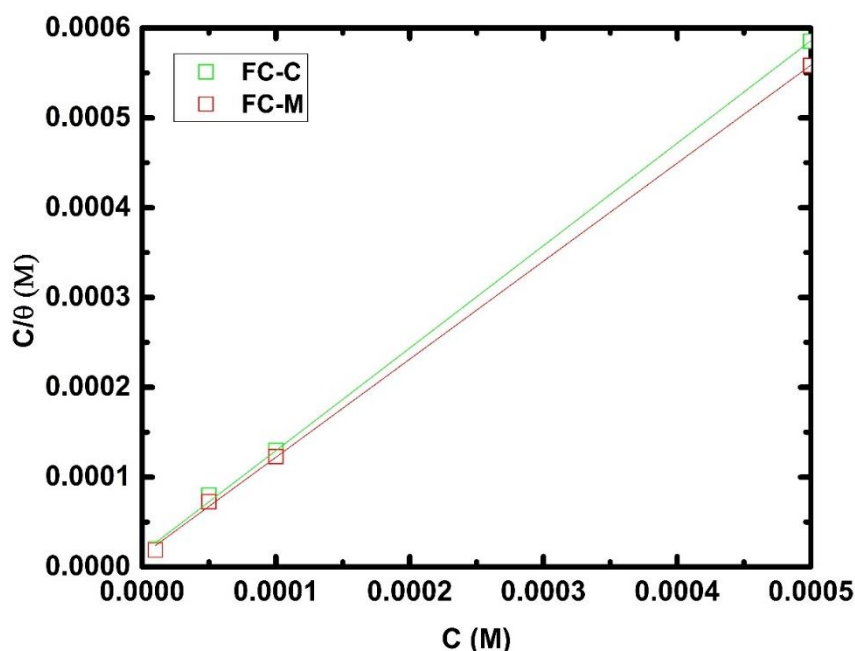
Figure 5. Plots of the Langmuir adsorption isotherm of furocoumarin derivatives at 303 K.

The Langmuir adsorption isotherm can be presented as follows:

$$\frac{C}{\theta} = \frac{1}{K_{ads}} + C \qquad (17)$$

where, θ is the surface coverage, C is the concentration of inhibitors and K_{ads} is the equilibrium constant of the adsorption process. K_{ads} is directly related to the standard free energy of adsorption (ΔG_{ads}^0) by the following equation:

$$\Delta G_{ads}^{\circ} = -RT \ln(K_{ads} \times 55.5) \qquad (18)$$

where, 55.5 is the molar concentration of water expressed in mol L^{-1}, R is the universal gas constant and T is the absolute temperature. The thermodynamic parameters are listed in Table 5. The linear regression coefficient ($R^2 = 0.99$) and the slope value are close to 1 which show that the adsorption of furocoumarins obeys Langmuir isotherm model. This means a monolayer adsorption on the metal surface along with the negligible interaction of adsorbed inhibitor molecules. The slight change in the values of ΔG_{ads}° for two tested inhibitors means that at equilibrium, both compounds can be adsorbed on

metal surface by almost equal extent[17]. The higher magnitudes of the adsorption-desorption equilibrium constant revealed that studied inhibitors had a high adsorption capacity on the surface of the mild steel. According to literature data [52,58], adsorption mechanism is generally classified into two types: chemisorption, $\Delta G^{\circ}_{ads} \sim -40$ kJ mol^{-1} or more negative, and physisorption, $\Delta G^{\circ}_{ads} \sim -20$ kJ mol^{-1} or less negative. The obtained ΔG^{0}_{ads} values for two inhibitor molecules are between -20 kJ mol^{-1} and -40 kJ mol^{-1}, which reflects mixed type of adsorption (both physisorption as well as chemisorption) taking place on the metallic surface [59].

Table 5. The adsorption parameters for the corrosion of MS in inhibited solutions at 303 K.

Inhibitor	Slope	K_{ads} (M^{-1})	R^2	ΔG°_{ads} (kJ mol^{-1})
FC-C	1.06	64688	0.999	-38
FC-M	1.04	77080	0.999	-39

3.5. DFT calculations

3.5.1. Global reactivity descriptors

During the last decade, the search for the relationship between electronic proprieties of corrosion inhibitors and their efficiencies has become a major area of interest in the corrosion inhibition field[60]. Density Functional Theory calculations were used as one of the most well-known tools for assessing the reactivity and selectivity parameters of inhibitor molecules[61]. Inhibitor molecules possess a variety of regions within themselves; this means that these regions have different tendencies of interactions with the surface of the metal. The reactivity and selectivity parameters can be utilized to determine and identify the molecular regions that have the tendency to react with the surface of the metal[62]. The reactivity of inhibitor compounds depends on the electronic properties such as electron density and partial charges on atoms, among others. These electronic properties have their influence from the type and nature of the functional groups that are within the inhibitor molecules[62]. Figure 6 shows the optimized geometries for the two compounds utilized in this study. The geometry of the molecules is of crucial importance during the selection of the inhibitor compounds because the inhibition efficiency also depends on the geometry of the compound. Compounds with planar geometry show better inhibition efficiency than those of less planar geometry [62]. Most of their atoms could be in contact with the metal substrate, whereas the ones with less planar geometry have a limited number of their atoms in contact with the surface of the metal during inhibitor-metal interactions.
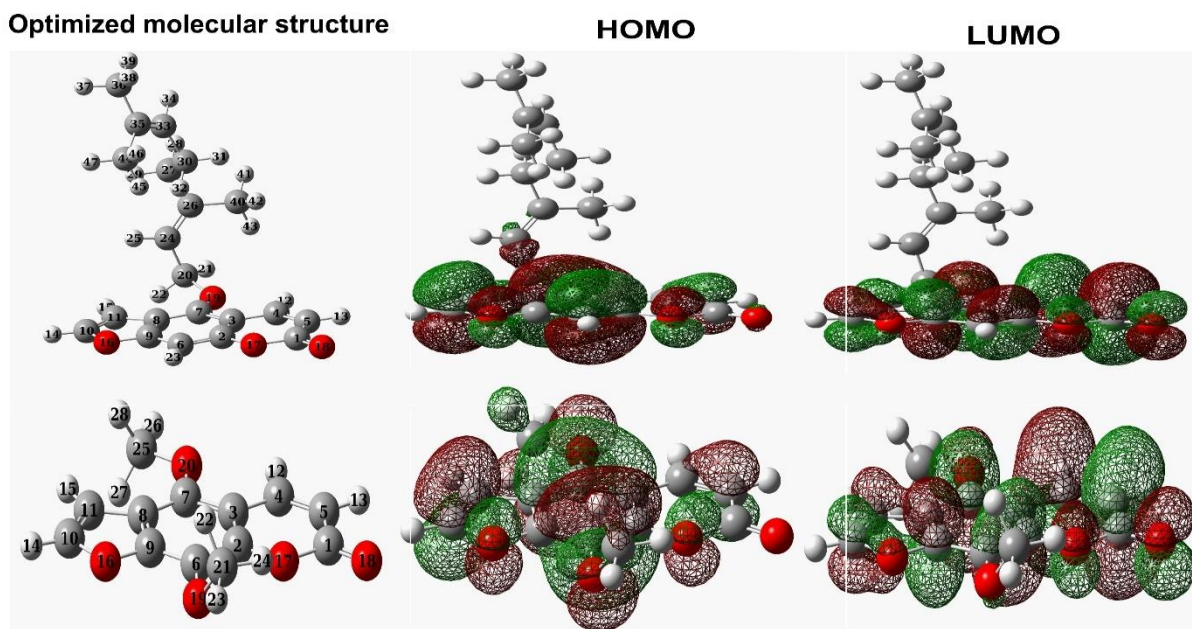
Figure 6. Optimized molecular structure and frontier orbitals distribution of furocoumarin derivatives.

The HOMO and LUMO orbitals could give us a more useful information to explain the mechanism of corrosion inhibition. The HOMO and LUMO orbital distributions of each of the studied furocoumarins are shown in Figure 6.

As it is well known, the frontier molecular orbitals, HOMO and LUMO may be used to predict the ability of inhibitor molecules to donate and accept electrons respectively [52]. Analysis of the HOMO densities shows that the highest HOMO densities occur almost on the entire molecular structure for both inhibitor molecules except of the carbon chain in FC-C. This result indicates that there are several preferred sites for electrophilic attack. The preference for the atoms in the aromatic ring to donate electrons to the metal atoms is related to the fact that the aromatic ring has π-electrons, which are available for donation to metal atoms. The HOMO density on the O atoms correspond to the lone pair of electrons in the non-bonding π-orbitals. The LUMO density distribution for both inhibitors shows that it is delocalized throughout inhibitor molecules except of the carbon chain in FC-C.

Table 6 reports the quantum chemical parameters that are related to the reactivity of inhibitors. These parameters include E_{HOMO}, E_{LUMO}, the energy gap ($\Delta E = E_{HOMO} - E_{LUMO}$) and fraction of electron transferred ΔN.

Table 6. The computed quantum chemical parameters for furocoumarin derivatives using DFT/B3LYB/6-311++G (d, p).

Inhibitors	E_{HOMO} (eV)	E_{LUMO} (eV)	ΔE_{gap} (eV)	ΔN_{110}
FC-C	-5.78	-1.52	4.26	0.273
FC-M	-5.60	-1.59	4.00	0.304

The molecular orbital theories of chemical reactivity such Frontier Molecular Orbital Theory (FMO) inform that the interactions between the HOMO and LUMO of reacting species is responsible for the transition of electron during the adsorption process between the MS surface and furocoumarin compounds[63]. The tendency regarding the donation of an electron by a molecule is normally measured by the E_{HOMO}. This means that higher values of E_{HOMO} are associated with a higher tendency to donate electrons by the molecule to the electron deficient species [62,64]. Thus, compounds possessing higher values of E_{HOMO} exhibit a better inhibition efficiency. Table 6 suggests that the inhibitor compound possessing the highest E_{HOMO} value is FC-M while the one with the lowest is FC-C. It is also very imperative to mention that the values of E_{HOMO} alone are not enough for us to draw conclusions with regard to the adsorbability of the compound on the surface of the metal, thus the inhibition efficiency. The LUMO energy can provide information about the tendency of an inhibitor molecule to accept an electron. Literature reveals that molecules possessing lower values of E_{LUMO} have a greater tendency to accept electrons from species that are electron rich[52]. From Table 6, it can be observed that FC-C has the highest value at -1.522 eV while FC-M is the lowest at -1.595 eV. Further details regarding the reactivity of these compounds towards the metal surfaces can be obtained through the investigation of the energy gap ΔE. The energy gap of the molecule can be directly related to its stability and consequently its tendency to react. Inhibitor molecules that exhibit low energy gap could be promising compounds for corrosion protection applications [65]. As reported in Table 6, FC-C and FC-M have the highest and lowest values of 4.26 eV and 4.0 eV, respectively.

3.5.2. Active sites

Beside molecular reactivity descriptors, quantum chemical studies can also provide information on the molecular selectivity parameters, which include Fukui functions. When an atom in a molecule possesses a tendency to donate an electron or a pair of electrons, that molecule is said to have a nucleophilic character while the one that has the tendency to accept electrons is said to have an electrophilic character[52]. The Fukui indices of all atomic sites were calculated and listed in Table 7. We notice from Table 7 that the C(1), C(4) and O(18) atoms of the compound FC-C and FC-M possess high values of f_k^+ indicating that these atoms are available to accept electrons from the metal surface (electrophilic etching). On the other hand, the C(6), C(10) and C(11) atoms of FC-C and the C(6), C(7) and O(19) atoms of FC-M possess high values of f_k^- which means that are responsible for the nucleophilic attack.

Table 7. The Fukui indices of the furocoumarin derivatives calculated AT DFT/GGA level.

	FC-C			FC-M	
Atom	f^+	f^-	Atom	f^+	f^-
C(1)	0.093	0.015	C(1)	0.097	0.021
C(2)	0.036	0.036	C(2)	0.046	0.065
C(3)	0.005	0.020	C(3)	0.002	0.037

|					
C(4)	0.141	0.007	C(4)	0.143	0.016
C(5)	0.076	0.024	C(5)	0.078	0.045
C(6)	0.041	0.063	C(6)	0.038	0.083
C(7)	0.078	0.041	C(7)	0.073	0.077
C(8)	0.006	0.036	C(8)	0.018	0.030
C(9)	0.040	0.023	C(9)	0.044	0.042
C(10)	0.027	0.068	C(10)	0.025	0.055
C(11)	0.022	0.049	C(11)	0.019	0.040
O(16)	0.024	0.026	O(16)	0.024	0.035
O(17)	0.041	0.021	O(17)	0.041	0.013
O(18)	0.099	0.031	O(18)	0.094	0.048
O(19)	0.029	0.027	O(19)	0.016	0.078
C(20)	-0.015	-0.005	O(20)	0.018	0.067
C(24)	0.001	0.013	C(21)	-0.010	-0.013
C(26)	0.002	0.013	C(25)	-0.009	-0.012
C(27)	0.001	-0.008			
C(30)	-0.005	-0.005			
C(33)	0.004	0.054			
C(35)	0.001	0.041			
C(36)	-0.000	-0.003			
C(40)	-0.001	-0.001			
C(44)	0.000	-0.003			

3.6. MD simulations

More recently, there has been a growing number of studies that have been published focusing on the simulation of the corrosion inhibition process[21]. In fact, molecular dynamic simulations have long been a question of great interest in this field[66]. Herein, only one inhibitor molecule was allowed to interact with iron surface in presence of solvent and corrosive particles like H_3O^+ and Cl^- ions. The MD outcomes at final configuration of the MD simulation box are shown in Figure 7.

At the end of the simulation process, both inhibitor molecules moved near the iron surface with flat or parallel disposition. The observed preference toward a parallel orientation would facilitate binding with the metal surface through multiple inhibitor-iron interactions such as donation and back-donation interactions. Table 8 shows both interaction and binding energies of tested inhibitors.
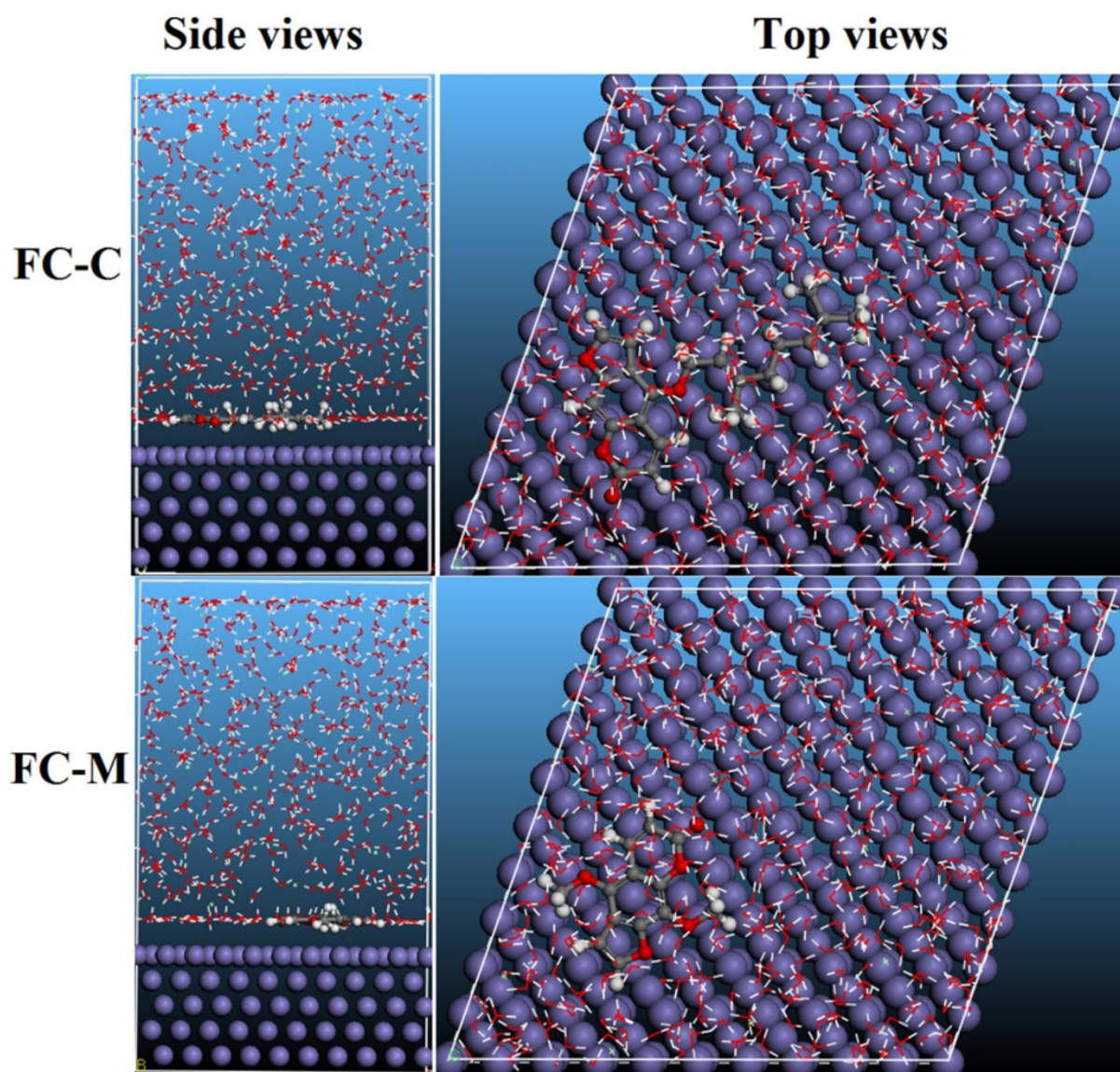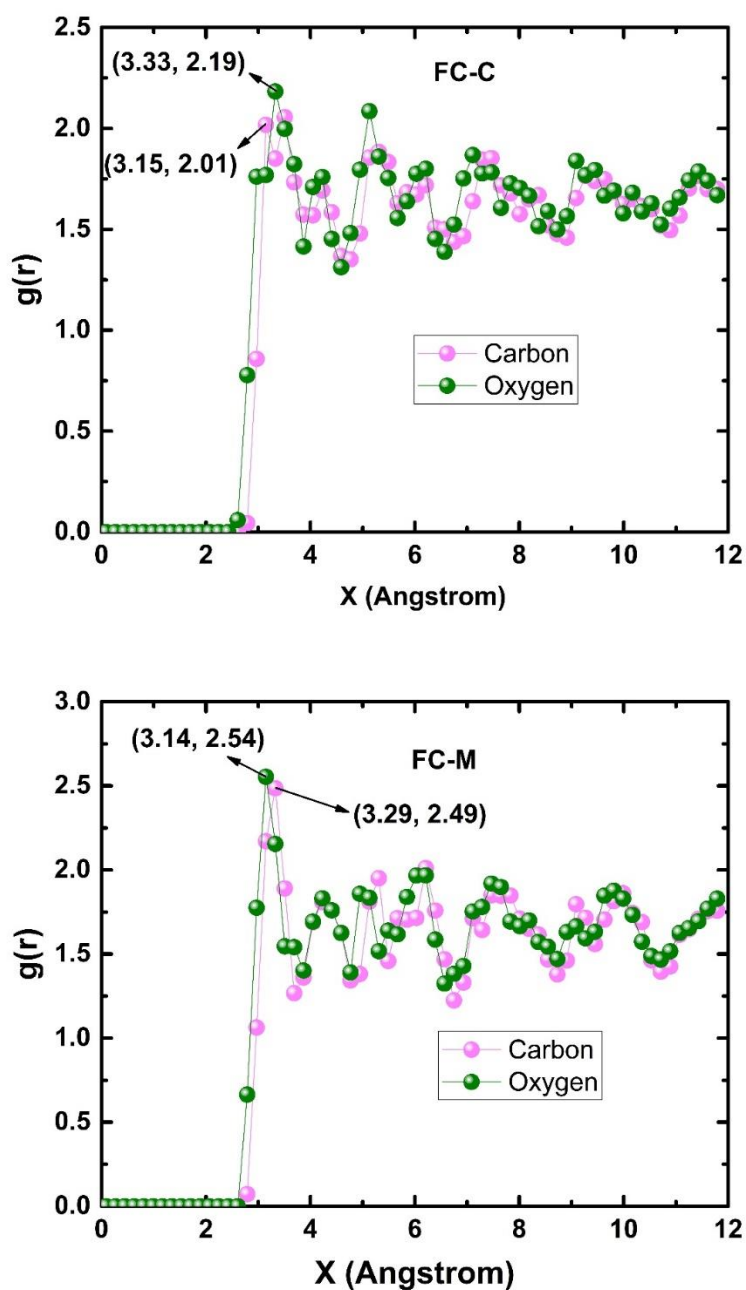
Figure 7. Side and top views of the final adsorption of furocoumarin derivatives on the Fe(110) surface in solution.

Table 8. Energy parameters obtained from MD simulations for adsorption of inhibitors on Fe (110) surface.

System	$E_{\text{interaction}}$ (kJ/mol)	E_{binding} (kJ/mol)
Fe + **FC-C** +491H$_2$O + $9H_3O^+$ + $9Cl^-$	-709.195	709.195
Fe + **FC-M** +491H$_2$O + $9H_3O^+$ + $9Cl^-$	-878.007	878.007

**Figure 8.** RDF analysis of FC-C and FC-M adsorbed on the surface of iron.

A larger binding energy implies a larger adsorption ability of inhibitor and thus typically higher inhibitive performance. The FC-M has a larger value of binding energy, showing that this inhibitor is more likely to be adsorbed on iron surface than FC-C, thus having a greater inhibitive action [67]. Considering these results, it is reasonable to consider what factors may account for the differences between the two inhibitors. Besides the presence of several oxygen atoms, inhibition potency seems to be related to the carbon chain length and methoxy groups of FC-C and FC-M respectively. These are in agreement with observations that compounds containing carbon chain and methoxy groups have good inhibition properties[68]. These results suggest again a potential role of the methoxy as a higher electron

donating group in increasing the interactive ability of corrosion inhibitors with the metal surface which ultimately results in an increased protection efficiency [69]. These factors may explain the observed experimental inhibition efficiency and are in good agreement with DFT studies.

Furthermore, radial distribution function (RDF) can shed new light on the nature of the interaction between iron surface and inhibitors. The radial distribution function was computed from MD simulations and it is used as useful method to judge the molecule–metal interaction types [68]. The typical bond length for chemisorption is 1 Å ~ 3.5 Å, while that of the physical adsorption is longer than 3.5 Å[22]. The RDFs of all non-hydrogen atoms are set out in Figure 8. In FC-C, the bonding length of Fe-C and Fe-O are 3.15 Å and 3.33 Å respectively. In FC-M, the bonding length of Fe-C and Fe-O are 3.29 Å and 3.14 Å respectively. These bonding lengths are all less than 3.5 Å, which suggest that significant interaction can be occurs between active sites of tested inhibitors and the iron surface. Interestingly, the bond length was observed to be almost similar in both compounds. RDF data support previous results showing the significant adsorption of tested compounds on the iron surface.

3.7. Scanning Electron Microscope

The surface morphology of the mild steel surface exposed to 1.0 M HCl without and with 5×10^{-4} M of FC-M for 24h was studied by scanning electron microscope. The results are shown in Figure 9. The surface of the mild steel in absence of inhibitor is highly corroded and damaged due to metal dissolution. In contrast, smoother surface was observed in the presence of inhibitor. The surface morphology remarkably improved due to better adsorption of inhibitor on the mild steel surface.
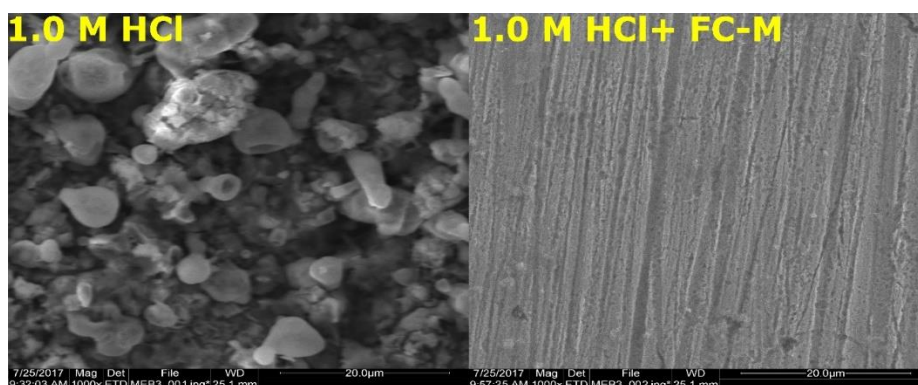

Figure 9. SEM images of MS in 1.0 M HCl alone and 1.0 M HCl + 5×10^{-4} M of FC-M after 24h of immersion time.

3.8. Mechanism of corrosion inhibition

Generally, the mechanism of actions of corrosion inhibitors on metal surface in acid medium is believed to be influenced by the chemical structure of the inhibitor molecules and the nature and charge of the metal. The presence of heteroatoms and functional groups ensures a strong interaction between metal surface and inhibitor molecules, thereby increasing film formation on metal. In this study, the results showed that tested furocoumarins act as good corrosion inhibitors for mild steel protection with

great electronic properties. According to obtained results, it can be hypothesized that the mechanism of adsorption of tested inhibitors can be explained by one and/or more of the following ways (Figure 10) [70,71].

(I) Corrosion inhibition experiments were carried out in HCl medium, which mostly leads to a positive charge of the metal surface. In this medium, an organic molecule is highly expected to be protonated. These conclusions are well recognized in many similar studies [72]. In such a situation, the neutral inhibitor molecule would be in equilibrium with its corresponding protonated form as follows[72] :

$$FCs + H^+ \Leftrightarrow (FCsH)^+ \qquad\qquad (20)$$
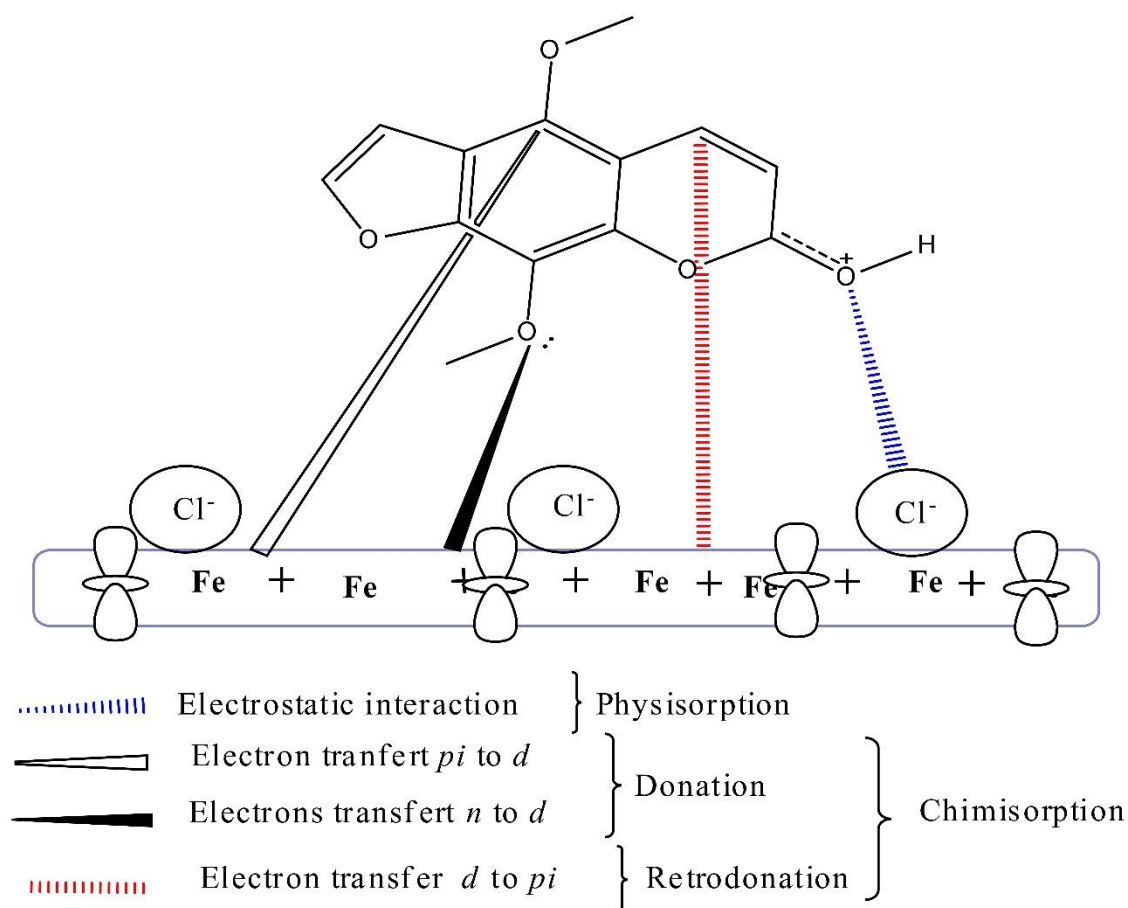
Figure 10. Pictorial representation of adsorption of FC-M on MS surface in 1.0 M HCl.

In the metal/electrolyte interface, chlorine ions, which preferentially adsorbed onto the steel surface work as intermediaries, creating a bridge between protonated inhibitor molecules and the charged metallic surface, i.e. electrostatic interactions.

(II) Then, inhibitor molecules create coordinate bonds with vacant d-orbitals of the metal [73] through unshared electron pair of heteroatoms and π-electrons of the aromatic ring.

(III) The strong transfer of electrons from inhibitor molecules to metal surface leads to an extra negative charge on steel surface. Electron back donation is believed to be responsible for the electron

transfer from metal surface to inhibitor molecules. Therefore, it has a more important impact on the strength of the bonding of organic molecules with Fe atoms.

4. CONCLUSION

Returning to objectives of this study, it is now possible to state that both natural compounds have good inhibitive properties for mild steel in 1.0 M HCl. Polarization studies have shown that the studied inhibitors work as mixed-type inhibitors. The adsorption of inhibitors on the mild steel surface obeys the Langmuir adsorption isotherm. Further insights on how inhibitor molecules adsorbed on the iron surface, were taken from MD simulations, radial distribution function and DFT studies. One of the strengths of this study is that it represents a comprehensive explanation of the corrosion inhibition mechanism of green furocoumarin compounds. Nevertheless, further research could also be conducted to determine the effectiveness of these compounds for the protection of other metals in varied environments.

References

1. Y. Zhang, Y. Cheng, F. Ma, K. Cao, *Int. J. Electrochem. Sci.* 14 (2019) 999.
2. F. Bentiss, M. Outirite, M. Traisnel, H. Vezin, M. Lagrenée, B. Hammouti, S.S. Al-Deyab, C. Jama, *Int. J. Electrochem. Sci.* 7 (2012) 1699.
3. M.A. Ameer, A.M. Fekry, A. Othman, *Int. J. Electrochem. Sci.* 9 (2014) 1964.
4. G. Khan, W.J. Basirun, A.B.B.M. Badry, S.N. Kazi, P. Ahmed, S.M. Ahmed, G.M. Khan, *Int. J. Electrochem. Sci.* 13 (2018) 12420.
5. X. Zhang, B. Tan, *Int. J. Electrochem. Sci*. 13 (2018) 11388.
6. H. Lgaz, R. Salghi, I.H. Ali, *Int. J. Electrochem. Sci*. 13 (2018) 250.
7. D. Dwivedi, K. Lepková, T. Becker, *RSC Adv*. 7 (2017) 4580.
8. P. Wadhwani, V. Panchal, N. Shah, *RSC Adv*. 6 (2016) 90897.
9. S. Pareek, D. Jain, S. Hussain, A. Biswas, R. Shrivastava, S.K. Parida, H.K. Kisan, H. Lgaz, I.-M. Chung, D. Behera, *Chem. Eng. J.* 358 (2019) 725.
10. V. Srivastava, J. Haque, C. Verma, P. Singh, H. Lgaz, R. Salghi, M.A. Quraishi, *J. Mol. Liq.* 244 (2017) 340.
11. A. Biswas, D. Das, H. Lgaz, S. Pal, U.G. Nair, *J. Mol. Liq.* 275 (2019) 867.
12. R. Kumar, S. Chahal, S. Kumar, S. Lata, H. Lgaz, R. Salghi, S. Jodeh, *J. Mol. Liq.* 243 (2017) 439.
13. D.I. Njoku, Y. Li, H. Lgaz, E.E. Oguzie, *J. Mol. Liq.* 249 (2018) 371.
14. A. Singh, K.R. Ansari, J. Haque, P. Dohare, H. Lgaz, R. Salghi, M.A. Quraishi, *J. Taiwan Inst. Chem. Eng.* 82 (2018) 233.
15. N. Saini, R. Kumar, H. Lgaz, R. Salghi, I.-M. Chung, S. Kumar, S. Lata, *J. Mol. Liq.* 269 (2018) 371.
16. N. Yilmaz, A. Fitoz, ÿmit Ergun, K.C. Emregül, *Corros. Sci.* 111 (2016) 110.
17. A. Dutta, S.K. Saha, P. Banerjee, D. Sukul, *Corros. Sci.* 98 (2015) 541.
18. C. Verma, E.E. Ebenso, I. Bahadur, M.A. Quraishi, *J. Mol. Liq*. 266 (2018) 577.
19. S.A. Umoren, U.M. Eduok, *Carbohydr. Polym.* 140 (2016) 314.
20. C. Verma, E.E. Ebenso, M.A. Quraishi, *J. Mol. Liq.* 233 (2017) 403.

21. Y. Yan, X. Wang, Y. Zhang, P. Wang, X. Cao, J. Zhang, *Corros. Sci.* 73 (2013) 123.
22. S.-W. Xie, Z. Liu, G.-C. Han, W. Li, J. Liu, Z. Chen, *Comput. Theor. Chem.* 1063 (2015) 50.
23. S.-Q. Hu, A.-L. Guo, Y.-G. Yan, X.-L. Jia, Y.-F. Geng, W.-Y. Guo, *Comput. Theor. Chem.* 964 (2011) 176.
24. S.G. Lee, K. Kim, T.M. Vance, C. Perkins, A. Provatas, S. Wu, A. Qureshi, E. Cho, O.K. Chun, *Int. J. Food Sci. Nutr.* 67 (2016) 881.
25. H. Dehghan, Y. Sarrafi, P. Salehi, S.N. Ebrahimi, *Med. Chem. Res.* 26 (2017) 849.
26. D. Chen, J. Yu, Chin *Tradit. Herb. Drugs* 17 (1986) 4.
27. E. Gopälakrishna, W. Watson, M. Bittner, M. Silva, *J. Chem. Crystallogr.* 7 (1977) 107.
28. H.E. Kleiner, S.V. Vulimiri, M.F. Starost, M.J. Reed, J. DiGiovanni, *Carcinogenesis,* 23 (2002) 1667.
29. M. Prince, C.T. Campbell, T.A. Robertson, A.J. Wells, H.E. Kleiner, *Carcinogenesis*, 27 (2005) 1204.
30. J. Scully, R. Baboian, *ASTM Phila. PA.* (1995) 110.
31. ASTM Committee G-1 on Corrosion of Metals, Standard practice for preparing, cleaning, and evaluating corrosion test specimens, *ASTM International,* 2011.
32. Z. Salarvand, M. Amirnasr, M. Talebian, K. Raeissi, S. Meghdadi, *Corros. Sci.* 114 (2017) 133.
33. J. Tkacz, J. Minda, S. Fintová, J. Wasserbauer, *Materials,* 9 (2016) 925.
34. aGA Petersson, A. Bennett, T.G. Tensfeldt, M.A. Al-Laham, W.A. Shirley, J. Mantzaris, *J. Chem. Phys.* 89 (1988) 2193.
35. C. Lee, W. Yang, R.G. Parr, *Phys. Rev. B.* 37 (1988) 785.
36. Z. Salarvand, M. Amirnasr, M. Talebian, K. Raeissi, S. Meghdadi, *Corros. Sci.* 114 (2017) 133.
37. R.G. Pearson, *Inorg. Chem.* 27 (1988) 734.
38. V. Sastri, J. Perumareddi, *Corrosion*, 53 (1997) 617.
39. Z. Cao, Y. Tang, H. Cang, J. Xu, G. Lu, W. Jing, *Corros. Sci.* 83 (2014) 292.
40. A. Kokalj, *Chem. Phys.* 393 (2012) 1.
41. Materials Studio, Revision 6.0, Accelrys Inc., San Diego, USA, 2013.
42. H. Mi, G. Xiao, X. Chen, *Comput. Theor. Chem.* 1072 (2015) 7.
43. S.K. Saha, P. Ghosh, A. Hens, N.C. Murmu, P. Banerjee, *Phys. E Low-Dimens. Syst. Nanostructures*, 66 (2015) 332.
44. L. Guo, I.B. Obot, X. Zheng, X. Shen, Y. Qiang, S. Kaya, C. Kaya, *Appl. Surf. Sci.* 406 (2017) 301.
45. H. Sun, *J. Phys. Chem. B.* 102 (1998) 7338.
46. S.K. Saha, A. Dutta, P. Ghosh, D. Sukul, P. Banerjee, *Phys. Chem. Chem. Phys.* 18 (2016) 17898.
47. J.-P. Hansen, I.R. McDonald, *Academic Press*, 2013.
48. A.K. Singh, S. Mohapatra, B. Pani, *J. Ind. Eng. Chem.* 33 (2016) 288.
49. M. Hegazy, A. Badawi, S.A. El Rehim, W. Kamel, *Corros. Sci.* 69 (2013) 110.
50. J. Aljourani, K. Raeissi, M. Golozar, *Corros. Sci.* 51 (2009) 1836.
51. H. Lgaz, R. Salghi, K. Subrahmanya Bhat, A. Chaouiki, Shubhalaxmi, S. Jodeh, *J. Mol. Liq.* 244 (2017) 154.
52. H. Lgaz, K. Subrahmanya Bhat, R. Salghi, Shubhalaxmi, S. Jodeh, M. Algarra, B. Hammouti, I.H. Ali, A. Essamri, *J. Mol. Liq.* 238 (2017) 71.
53. B. Hirschorn, M.E. Orazem, B. Tribollet, V. Vivier, I. Frateur, M. Musiani, *Electrochimica Acta,* 55 (2010) 6218.
54. E. Alibakhshi, E. Ghasemi, M. Mahdavian, B. Ramezanzadeh, S. Farashi, *J. Taiwan Inst. Chem. Eng.* 75 (2017) 248.
55. M. Gholami, I. Danaee, M.H. Maddahy, M. RashvandAvei, *Ind. Eng. Chem. Res.* 52 (2013) 14875.
56. C. Verma, E. Ebenso, I. Bahadur, I. Obot, M. Quraishi, *J. Mol. Liq.* 212 (2015) 209.
57. M. Yadav, R.R. Sinha, T.K. Sarkar, N. Tiwari, *J. Adhes. Sci. Technol.* 29 (2015) 1690.
58. M. Yadav, D. Behera, S. Kumar, R.R. Sinha, *Ind. Eng. Chem. Res.* 52 (2013) 6318.

59. H. Lgaz, R. Salghi, S. Jodeh, B. Hammouti, *J. Mol. Liq.* 225 (2017) 271.
60. I. Obot, N. Obi-Egbedi, E. Ebenso, A. Afolabi, E. Oguzie, *Res. Chem. Intermed.* 39 (2013) 1927.
61. M. Shahraki, M. Dehdab, S. Elmi, *J. Taiwan Inst. Chem. Eng.* 62 (2016) 313.
62. Z. Cao, Y. Tang, H. Cang, J. Xu, G. Lu, W. Jing, *Corros. Sci.* 83 (2014) 292.
63. A. Tazouti, M. Galai, R. Touir, M.E. Touhami, A. Zarrouk, Y. Ramli, M. Saraçoğlu, S. Kaya, F. Kandemirli, C. Kaya, *J. Mol. Liq.* 221 (2016) 815.
64. Z. Salarvand, M. Amirnasr, M. Talebian, K. Raeissi, S. Meghdadi, *Corros. Sci.* 114 (2017) 133.
65. M. Messali, H. Lgaz, R. Dassanayake, R. Salghi, S. Jodeh, N. Abidi, O. Hamed, *J. Mol. Struct.* 1145 (2017) 43.
66. J. Zhang, W. Yu, L. Yu, Y. Yan, G. Qiao, S. Hu, Y. Ti, *Corros. Sci.* 53 (2011) 1331.
67. J. Zhou, S. Chen, L. Zhang, Y. Feng, H. Zhai, *J. Electroanal. Chem.* 612 (2008) 257.
68. D. Zhang, Y. Tang, S. Qi, D. Dong, H. Cang, G. Lu, *Corros. Sci.* 102 (2016) 517.
69. K.R. Ansari, M.A. Quraishi, A. Singh, *J. Ind. Eng. Chem.* 25 (2015) 89.
70. N.K. Gupta, C. Verma, M.A. Quraishi, A.K. Mukherjee, *J. Mol. Liq.* 215 (2016) 47.
71. C. Verma, E.E. Ebenso, I. Bahadur, I.B. Obot, M.A. Quraishi, *J. Mol. Liq*. 212 (2015) 209.
72. R. Yıldız, T. Doğan, İ. Dehri, *Corros. Sci.* 85 (2014) 215.
73. L. Tang, X. Li, L. Li, G. Mu, G. Liu, *Mater. Chem. Phys.* 97 (2006) 301.